FEBRUARY 01 2008

An improved acoustical wave propagator method and its application to a duct structure

S. Z. Peng; L. Cheng

J. Acoust. Soc. Am. 123, 610–621 (2008)
https://doi.org/10.1121/1.2821971

An improved acoustical wave propagator method and its application to a duct structure

S. Z. Peng[a] and L. Cheng
Department of Mechanical Engineering, The Hong Kong Polytechnic University, Hung Hom, Kowloon, Hong Kong

(Received 16 May 2007; accepted 12 November 2007)

The pseudospectral time-domain method has long been used to describe the acoustical wave propagation. However, due to the limitation and difficulties of the fast Fourier transform (FFT) in dealing with nonperiodic problems, the dispersion error is inevitable and the numerical accuracy greatly decreases after the waves arrive at the boundary. To resolve this problem, the Lagrange–Chebyshev interpolation polynomials were used to replace the previous FFT, which, however, brings in an additional restriction on the time step. In this paper, a mapped Chebyshev method is introduced, providing the dual benefit of preserving the spectral accuracy and overcoming the time step restriction at the same time. Three main issues are addressed to assess the proposed technique: (a) Spatial derivatives in the system operator and the boundary treatment; (b) parameter selections; and (c) the maximum time step in the temporal operator. Furthermore, a numerical example involving the time-domain evolution of wave propagation in a duct structure is carried out, with comparisons to those obtained by Euler method, the fourth-order Runge–Kutta method, and the exact analytical solution, to demonstrate the numerical performance of the proposed technique.
 [DOI: 10.1121/1.2821971]

PACS number(s): 43.20.Mv, 43.20.Bi [DSB] Pages: 610–621

I. INTRODUCTION

Partial differential equations (PDEs) describe a wide variety of physical processes such as molecular dynamics, heat conduction, flow, and sound propagation. Over the last decade, a great deal of effort has been devoted to the development of numerical methods for solving the time-dependent PDEs, in particular the time-dependent Schrödinger equation and wave equations.[1–8] Since the time-domain investigation provides insightful understanding on the governing physical phenomena, various numerical schemes have been developed in parallel in many fields by quantum chemists, quantum physicists, and acousticians with little across referencing. Typical numerical methods include the finite-difference time-domain, finite-element time-domain, and time-domain boundary-element method for modeling and simulating molecular encounters, calculating the dynamical properties of a quantum mechanical system including molecular dynamics, and for predicting transient wave propagation and scattering problems.[9,10]

Consider a wave function ψ governed by the time-dependent Schrödinger equation,[11]

$$i\frac{\partial}{\partial t}\psi(x,t) = H\psi(x,t), \tag{1}$$

where

$$H = \underbrace{p^2/2m}_{K} + V$$

is the Hamiltonian operator; K and V the kinetic and potential operators, respectively; and p and m are the momentum and mass, respectively.

The solution of Eq. (1), with H independent of time, is given by

$$\psi(x,t+\tau) = e^{-iH\tau}\psi(x,t), \tag{2}$$

where $\hat{Q}=e^{-iH\tau}$ denotes the quantum wave propagator, which maps the wave function $\psi(x,t)$ at any time t to that at next time $t+\tau$.

To implement the operation of the exponential propagator, $\hat{Q}$ is often approximated to a finite polynomial expansion. A comprehensive discussion on various expansion schemes can be found in the review article by Balakrishnan *et al.*[12] It is worth noting that Kosloff and Tal-Ezer[13–15] did a pioneering work on the pseudospectral method in the field of quantum chemistry and atomic physics, which is an important step in developing time-domain numerical methods. In particular, they described a Chebyshev expansion of the evolution operator as an efficient and accurate method for calculating the time-dependent Schrödinger equation. After that, they proposed a modified Chebyshev pseudospectral method with an $O(N^{-1})$ time step restriction, which was the main drawback in restrictive stability properties.[16] Don and Solomonoff[17] studied a similar method in reducing the round-off error and calculated spatial derivatives using Chebyshev collocation methods. Leforestier *et al.*[18] discussed the advantages and drawbacks of several numerical methods in terms of the numerical accuracy, computational efficiency, and stability. Therefore, it is not surprising that great effort has been devoted to finding the optimum numerical method with an efficient, accurate, and stable numerical procedure to solve the time-dependent PDEs. Recently, Pan

[a]Author to whom correspondence should be addressed. Electronic mail: mmszpeng@polyu.edu.hk

and Wang[19] developed an explicit acoustical wave propagator (AWP) method to describe the time-domain evolution of acoustical waves. The Fourier transform scheme and the modified Bessel function of the first kind were used to evaluate the spatial derivatives, and to implement the acoustical wave propagator $e^{-\hat{H}\tau}$, respectively. The main difference between the quantum wave propagator $e^{-iH\tau}$ and the acoustical wave propagator $e^{-\hat{H}\tau}$ is that the former is complex while the latter is real in a matrix form representing the selected variables.

Examining the spatial and temporal discretization of the method shows that it is necessary to use a higher-order time differencing scheme to save computational time (by an increase in the time step size). The numerical accuracy of the method can be ensured by a good approximation of the spatial derivatives and the temporal exponential. Theoretically speaking, if $e^{-(t-t_0)\hat{H}}$ can be implemented together with the known initial-value vectors $\psi(x,t_0)$, then the above-mentioned AWP method can be used to predict the acoustical wave propagation like the exact analytical solutions [the order of the prediction error in dimensionless form is around $O(10^{-7})$] in Refs. 20–22. However, most practical engineering applications involve complex boundary conditions that need to be properly treated. Therefore, the existing problem is that the previous AWP method including the Fourier transform scheme can hardly deal with the nonperiodic problems such as asymmetrical boundary conditions.

More recently, as a further development of the AWP method, Peng and Huang[23] introduced the Lagrange–Chebyshev interpolation polynomials (by fully considering the boundary conditions) to replace the previous Fourier transform scheme in the implementation of the AWP. Despite the improvement on the spatial derivatives, however, the additional restriction on the time step is still left to be solved. The present paper aims to eliminate this restriction by remapping one set of points with Chebyshev–Gauss–Lobatto points to another set of points with the modified Chebyshev–Gauss–Lobatto points. By choosing an optimal parameter γ in the mapped Chebyshev method, a larger time step with higher computational efficiency and stability can be achieved. It is worth noting that the most distinct feature of the Chebyshev polynomial expansion scheme (still kept in this implementation of the AWP) is that the maximum polynomial expansion order n can be chosen such that the numerical accuracy is dominated by the machine accuracy of the computer, and the error is uniformly distributed over all the range of eigenvalues. The proposed method is essentially a transition between Fourier (γ=0) and Chebyshev spatial discretization methods.

The outline of the paper is as follows. In Sec. II, we derive an explicit AWP, which includes acoustical waves in a one-dimensional duct structure. Section III introduces the Lagrange–Chebyshev interpolation polynomials scheme for spatial derivatives, describes the treatment of nonperiodic/periodic boundary conditions, implements the AWP with the Chebyshev polynomial expansion, and studies the Fourth-order Kunge–Kutta (RK4) method and the mapped Chebyshev method. In Sec. IV, a numerical example is presented to carry out the error analysis together with the relevant maximum time step. Then the numerical performance (numerical accuracy, computational efficiency, and stability) of the improved AWP scheme is demonstrated. Finally, conclusions are drawn in Sec. V.

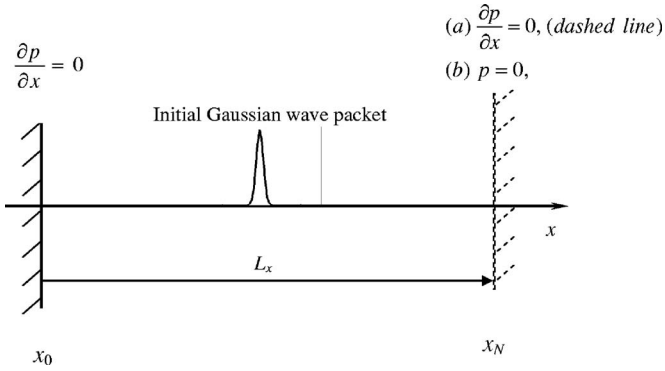

FIG. 1. Illustration of a duct structure with the initial-boundary-value problems: (a) Periodic boundaries (both rigid walls) and (b) nonperiodic boundaries (the left-hand side is rigid wall, the right hand side is pressure release wall).

II. A DUCT STRUCTURE MODEL AND THE AWP

The theoretical model under investigation consists of a one-dimensional duct structure (Fig. 1) with two different boundaries: (a) Periodic (rigid walls at both ends) and (b) nonperiodic (the left-hand side is a rigid wall, with the right-hand side being a pressure-release wall). Given an external sound source $P(x,t)$, the wave will propagate inside the duct.

Acoustical wave motion in the duct is described by the following partial differential equations (PDEs):

$$\frac{\partial p}{\partial t} = -\rho_0 c_0^2 \frac{\partial V}{\partial x},$$

$$\frac{\partial V}{\partial t} = -\frac{1}{\rho_0}\frac{\partial p}{\partial x}, \tag{3}$$

where ρ_0 is the air density; c_0 the speed of sound; p the sound pressure; and V the particle velocity along the x direction in the duct.

To derive the acoustical wave propagator in the duct, a state vector ϕ_D consisting of sound pressure p and particle velocity V is formed, transforming Eq. (3) into the following state equation:

$$\frac{\partial}{\partial t}\underbrace{\begin{bmatrix} p \\ V \end{bmatrix}}_{\phi_D} = -\hat{H}_D \begin{bmatrix} p \\ V \end{bmatrix}, \tag{4}$$

(4)where

$$\hat{H}_D = \begin{bmatrix} 0 & \rho_0 c_0^2 \frac{\partial}{\partial x} \\ \frac{1}{\rho_0}\frac{\partial}{\partial x} & 0 \end{bmatrix}. \tag{5}$$

Integrating Eq. (4) with respect to time yields

$$\phi_D(x,t) = e^{-(t-t_0)\hat{H}_D}\phi_D(x,t_0), \tag{6}$$

where $e^{-(t-t_0)\hat{H}_D}$ is defined as the AWP in a one-dimensional duct structure with the subscript D denoting the duct structure.

The numerical solution of Eq. (4) includes both the first-order spatial and temporal derivatives. When the initial values $\phi_D(x,t_0)$ are known, there are two key steps to obtain $\phi_D(x,t)$: (a) to calculate the spatial derivatives in $\hat{H}_D$ and (b) to adopt an efficient and accurate method to implement the exponential expansion $e^{-(t-t_0)\hat{H}_D}$.

III. CALCULATION OF THE SPATIAL DERIVATIVES AND IMPLEMENTATION OF THE AWP

As a class of methods, pseudospectral methods are used in solving the above-mentioned PDEs. The Fourier transform is often involved in the calculation of the spatial derivatives. For well-behaved problems (isotropic medium, symmetrical structure with periodic boundary conditions), the Fourier transform is very useful to evaluate the spatial derivatives due to its numerical accuracy and computational efficiency,

$$F\left[\frac{\partial'''}{\partial x'''}\psi(x,t)\right] = (jk_x)'''F[\psi(x,t)], \quad \frac{\partial'''}{\partial x'''}\psi(x,t) = F^{-1}\{(jk_x)'''F[\psi(x,t)]\}, \tag{7}$$

where $F[\ ]$ and $F^{-1}\{\ \}$ denote the Fourier and inverse Fourier transforms, respectively, and k_x is the wave number. The spatial approximation for the derivatives utilizes the property of the Fourier transforms that a derivative in the spatial domain becomes a multiplication by ik_{x_l} (k_{x_l} is the wave number corresponding to the l-spatial coordinate) in the spatial frequency domain, and then performs an inverse Fourier transform back to the spatial domain, as described in Eq. (7).

In the finite-difference and finite-element methods, time and space are discretized with a uniform grid. Typically, they do not attain good convergence even for an infinitely smooth function. Note the differences between the Fourier transform and the finite-difference method: The former is based on global approximations; and the latter on local approximations based on Taylor expansion, which is accompanied by the truncation errors. However, the numerical errors in the Fourier transform scheme are mainly due to the approximation of double integrals described in a discrete form. More precisely, the Fourier transform scheme can obtain very small truncation errors (high accuracy) by the positive and negative value cancellation in a global error summation except for two end points. It is observed that when the grid spacing Δx is small, the Fourier transform scheme has much higher accuracy than the multipoint finite-difference methods.

The above-mentioned discrete Fourier transform scheme implies periodic boundaries, which are natural for describing spatially periodic problems. However, for problems where the natural boundary conditions are nonperiodic, the Fourier transform scheme will introduce additional numerical dispersion and the numerical accuracy rapidly deteriorates. When this dispersion becomes too severe, the solutions to Eq. (2) no longer exist. The stability concern actually limits these explicit methods (Euler and RK4 methods) to small Δt except for the Chebyshev polynomial expansion scheme, where the time step Δt is mainly dependent on the parameter $R = dt|\lambda_{\max}|$, and normalized matrix $\hat{H}'_D$. For different structures, the system operator $\hat{H}$ has different forms leading to different maximum eigenvalues $\lambda_{\max}$. For example, for the sound pressure in a one-dimensional duct, $R = c_0\Delta t\pi/\Delta x$; for flexural waves in a thin flexible beam, $R = \sqrt{EI/\rho A}(\pi/\Delta x)^2 dt$.

A. Lagrange–Chebyshev interpolation polynomials scheme for spatial derivatives

In Eq. (5), there are two first-order spatial derivatives for sound pressure $\partial p(x,t)/\partial x$ and the particle velocity $\partial V(x,t)/\partial x$. For simplification, only the former $\partial p(x,t)/\partial x$ is derived as follows. The latter can be treated in a similar way.

Usually, the Chebyshev pseudospectral method is based on polynomial interpolation in the canonical interval $[-1,1]$. However, it can be defined on any finite internal $[x_0,x_N]$ for a general case by means of a linear transform of variable χ which maps $x \in [x_0,x_N]$ onto $[-1,1]$,

$$x = \frac{x_N - x_0}{2}\chi + \frac{x_N + x_0}{2}, \tag{8}$$

which is discretized at Gauss–Lobatto points $\chi_i = \cos[(N-i)\pi/N]$, $i = 0,1,\ldots,N$.

In this scheme, $\partial/\partial\chi$ is represented by a matrix $d_\chi = [d_{i,k}]$ with its elements $d_{i,k}$ given in the following (Ref. 23):

$$d_\chi = \begin{bmatrix} -\frac{2N^2+1}{6} & -\frac{2}{\chi_0-\chi_1} & \cdots & \frac{2(-1)^{N-1}}{\chi_0-\chi_{N-1}} & \frac{(-1)^N}{\chi_0-\chi_N} \\ -\frac{1}{2(\chi_1-\chi_0)} & -\frac{\chi_1}{2(1-\chi_1^2)} & \cdots & \frac{(-1)^N}{\chi_1-\chi_{N-1}} & \frac{(-1)^{N+1}}{2(\chi_1-\chi_N)} \\ \vdots & \vdots & \ddots & \vdots & \vdots \\ \frac{(-1)^{N-1}}{2(\chi_{N-1}-\chi_0)} & \frac{(-1)^N}{(\chi_{N-1}-\chi_1)} & \cdots & -\frac{\chi_{N-1}}{2(1-\chi_{N-1}^2)} & \frac{(-1)^{2N-1}}{2(\chi_{N-1}-\chi_N)} \\ \frac{(-1)^N}{\chi_N-\chi_0} & \frac{2(-1)^{N+1}}{\chi_N-\chi_1} & \cdots & \frac{2(-1)^{2N-1}}{\chi_N-\chi_{N-1}} & \frac{2N^2+1}{6} \end{bmatrix}. \tag{9}$$

The spatial derivative of a discretized function is given as

$$\frac{\partial\tilde{p}(\chi,t)}{\partial\chi} = \sum_{k=0}^{N} d_{i,k}\tilde{p}_k(\chi,t), \tag{10}$$

which can also be expressed as $[\partial\tilde{p}(\chi,t)/\partial\chi] = d_\chi[\tilde{p}(\chi,t)]$, where $[\partial\tilde{p}(\chi,t)/\partial\chi]$ and $[\tilde{p}(\chi,t)]$ are column matrices for the $(N+1)$ discrete points.

Theoretically, mth-order spatial derivatives $d_\chi^{(m)}$ can be obtained by the matrix product of

$$\underbrace{d_\chi^{(1)} \times d_\chi^{(1)} \times \cdots \times d_\chi^{(1)}}_{m}$$

[$d_z^{(1)} = d_\chi$ in Eq. (9)]. When $N+1$ grid points in χ axis are given, according to the relations between $x \in [x_0,x_N]$ and χ

$\in[-1,1]$, $\partial\tilde{p}(x,t)/\partial x$ can be obtained by multiplying $\partial\tilde{p}(\chi,t)/\partial\chi$ with the constant $2/(x_N-x_0)$.

B. Nonperiodic/periodic boundary conditions

A mathematical model with nonperiodic boundary conditions is introduced to describe how the boundary conditions are considered in the spatial derivatives. Here, as shown in Fig. 1, two different boundary conditions are considered: A rigid wall with $\partial\tilde{p}(x,t)/\partial x=0\Leftrightarrow\partial\tilde{p}(\chi,t)/\partial\chi=0$ is imposed on the left-hand side and a pressure-release wall with $\tilde{p}(x,t)=0$ is used on the right-hand side. The procedure is described as follows: (a) All values at the initial condition $\phi_D(x,t_0)$ are known, so $\partial\tilde{p}(x,t_0)/\partial x$ [obtained from $\partial\tilde{p}(\chi,t_0)/\partial\chi$] can be calculated; (b) the values at the new time step t_0+dt can be obtained by using $\phi_D(x,t_0+dt)=e^{-dt\hat{H}}\phi_D(x,t_0)$ for all inner points; then $\partial\tilde{p}(x,t_0+dt)/\partial x$ should be recalculated from $\partial\tilde{p}(\chi,t_0+dt)/\partial\chi$; and (c) the boundary conditions are applied to get $\phi_D(x,t_0+dt)$ on all boundaries. For example, the sound pressure $\tilde{p}(x_0,t_0+dt)$ and its spatial derivative on the left-hand side (rigid wall) are calculated by

$$\tilde{p}(x_0,t_0+dt)=-\Big(d_{0,1}\tilde{p}(x_1,t_0+dt)+\cdots+d_{0,N-1}\tilde{p}(x_{N-1},t_0+dt)+d_{0,N}\underbrace{\tilde{p}(x_N,t_0+dt)}_{=0}\Big)\Big/d_{0,0}, \tag{11}$$

and

$$\partial\tilde{p}(x_N,t_0+dt)/\partial x=2\Big(d_{N,0}\tilde{p}(x_0,t_0+dt)+\cdots+d_{N,N-1}\tilde{p}(x_{N-1},t_0+dt)+d_{N,N}\underbrace{\tilde{p}(x_N,t_0+dt)}_{=0}\Big)\Big/(x_N-x_0), \tag{12}$$

where $\tilde{p}(x_0,t_0+dt)$ in Eq. (12) should be obtained from Eq. (11). Spatial derivatives on the boundaries are calculated by the product of the Chebyshev derivative matrix with the acoustical quantity in the whole field.

Similarly, periodic boundary conditions [rigid wall conditions with $\partial\tilde{p}(x,t)/\partial x=0\Leftrightarrow\partial\tilde{p}(\chi,t)/\partial\chi=0$ imposed on both the left-hand and right-hand sides] should be fully considered in the spatial derivatives. The sound pressures $\tilde{p}(x_0,t_0+dt)$ and $\tilde{p}(x_N,t_0+dt)$ on the left-hand and right-hand sides are, respectively, calculated by

$$\tilde{p}(x_0,t_0+dt)=-\left((d_{0,1}d_{N,N}-d_{0,N}d_{N,1})\tilde{p}(x_1,t_0+dt)+\cdots+(d_{0,N-1}d_{N,N}-d_{0,N}d_{N,N-1})\tilde{p}(x_{N-1},t_0+dt)\right)/(d_{0,0}d_{N,N}-d_{0,N}d_{N,0}),$$

$$\tilde{p}(x_N,t_0+dt)=\left((d_{0,1}d_{N,0}-d_{0,0}d_{N,1})\tilde{p}(x_1,t_0+dt)+\cdots+(d_{0,N-1}d_{N,0}-d_{0,0}d_{N,N-1})\tilde{p}(x_{N-1},t_0+dt)\right)/(d_{0,0}d_{N,N}-d_{0,N}d_{N,0}). \tag{13}$$

It should be noted that the above-mentioned procedures are entirely explicit.

C. Chebyshev polynomial expansion schemes with *I* or *J* expansions

It is worth noting that the strategy chosen for the propagating scheme is to expand the evolution operator $AWP=e^{-\hat{H}_d dt}$ in a polynomial series. This strategy becomes a choice of the best polynomial approximation for this series, and the operator $e^{-(t-t_0)\hat{H}_D}$ on the initial wave packet can then be evaluated. The most accurate and stable method to date is the Chebyshev polynomial expansion scheme, which is used to implement the temporal approximation of the exponential propagator $e^{-(t-t_0)\hat{H}_D}$. Since the argument of these polynomials in $\phi_D(x,t)$ is defined in the range of $[-1,1]$, one needs to normalize the system operator $\hat{H}_D$ by $\hat{H}'_D=\hat{H}_D/|\lambda_{\max}|$, where $\lambda_{\max}$ denotes the maximum eigenvalue of $\hat{H}_D$. It is worth noting that the time-domain Chebyshev polynomial expansion scheme has the potential to keep a low error with very large time steps, which will be described in Sec. IV B.

The Chebyshev polynomial expansion schemes with *I* and *J* expansions can be used to expand the acoustical wave propagator. Their respective advantages and existing problems will be discussed in the following.

Denoting $R=(t-t_0)|\lambda_{\max}|$, Eq. (6) can be presented by

$$\phi_D(x,t)=\left[I_0(R)\underbrace{I}_{T_0(\hat{H}'_D)}+2I_1(R)\underbrace{\hat{H}'_D}_{T_1(\hat{H}'_D)}+2\sum_{n=2}^{\infty}I_n(R)T_n(\hat{H}'_D)\right]\phi_D(x,t_0), \tag{14}$$

where I is a unit matrix with the same size as that of $\hat{H}'_D$; $I_n(R)$ is the nth-order modified Bessel function of the first kind; and $T_n(\hat{H}'_D)$ is the nth-order Chebyshev polynomials, which can be calculated by the following recursive relations: $T_n(\hat{H}'_D)=2\hat{H}'_D T_{n-1}(\hat{H}'_D)-T_{n-2}(\hat{H}'_D)$, where $n\geqslant 2$. The main advantage of the Chebyshev polynomial expansion schemes with *I* expansion is that expansion coefficients of Chebyshev polynomials decay exponentially when the order of the coefficient function is sufficiently larger than its argument R, which is the important parameter as function of the size of time step and the maximum eigenvalue of the system operator.

However, the existing problem of the *I* expansion with the modified Bessel functions is that there is a limitation due to the dynamic range of expansion functions covered by a single AWP propagation [for a large R, $I_0(30)=7.8\times10^{11}$ comes close to the dynamic range of 10^{16}]. Therefore, the Bessel functions of the first kind, as an alternative expansion, are considered to replace the previous modified Bessel functions of the first kind. Thus, Eq. (6) can be represented by

$$\phi_D(x,t)=\left[J_0(R)\tilde{T}_0(\hat{H}'_D)+2J_1(R)\tilde{T}_1(\hat{H}'_D)+2\sum_{m=2}^{M}J_m(R)\tilde{T}_m(\hat{H}'_D)\right]\phi_D(x,t_0), \tag{15}$$

where $J_m(R)$ is the mth-order Bessel function of the first kind

and $\tilde{T}_m(\hat{H}'_D)$ is the mth-order Chebyshev polynomials, which can be calculated by the following recursive relations: $\tilde{T}_m(\hat{H}'_D)=2\hat{H}'_D\tilde{T}_{m-1}(\hat{H}'_D)-\tilde{T}_{m-2}(\hat{H}'_D)$, where $m\geqslant 2$.

The number of terms in the expansions (15) are governed by the behavior of the Bessel function $J_m(R)$. Equation (15) indicates the orthogonality properties that justify the expansion. When $R=1$, the expansion coefficients decay quickly. As R increases, different from the previous $I_n(R)$, the main advantage of the Chebyshev polynomial expansion schemes with J expansion is that expansion coefficients $J_m(R)$ are only bounded in $[-0.5,0.5]$ for $R=5$ and $[-0.2,0.2]$ for $R=50$. Once again, for large R values, the J expansion is better because large prediction errors can be avoided when some extra terms fall outside the dynamic range defined by the machine accuracy of the computer (10^{-16}). However, for small R values, the previous I expansion is strongly recommended due to its exponential decaying property. At the expense of sacrificing computational efficiency, high accuracy can be further achieved by the time-step splitting method ($e^{-R\hat{H}'_D}=\exp(-\Sigma_{m=1}^{M_R}(R/M_R)\hat{H}'_D)$, where the splitting slice $e^{-(R/M_R)\hat{H}'_D}$ can preserve sufficient prediction accuracy) introduced in Ref. 20.

A proper expansion scheme and the relevant optimal parameters hold the key to achieve accurate prediction results efficiently. Theoretically speaking, if the I expansion is selected, one can choose any large R with enough expansion term $n_{\min}$ to ensure that $I_0(R)/I_{n_{\min}}(R)$ reaches the order of 10^{-16}. However, due to the limitation of the dynamic range (increasing R is accompanied by the increased prediction error in the calculation), R should be chosen in a safety range to ensure its numerical accuracy. If possible, a smaller R is better to get the highly accurate prediction results. When R is given, the expansion term n will significantly affect the prediction results. Therefore, there exists an optimal selection among the time step dt and the minimum expansion term $n_{\min}$, which is very complex compared with the following RK4 method.

The main difference between the present improvement and the previous AWP method in Ref. 20 is that $[\partial\tilde{p}(\chi,t)/\partial\chi]=d_\chi[\tilde{p}(\chi,t)]\rightarrow[\partial\tilde{p}(x,t)/\partial x]=2d_\chi[\tilde{p}(\chi,t)]/(x_N-x_0)$ is included in $\hat{H}'_D$ to replace $F[\partial\tilde{p}(x,t)/\partial x]=ik_xF[\tilde{p}(x,t)]$ included in $\hat{H}'_D$. Once again, the former is nonuniform distribution of Chebyshev–Gauss–Lobatto points, but the latter is uniform distribution of points.

For a fixed step size, the Runge–Kutta method is regarded as a classical technique for the solution of differential equations, especially ordinary differential equations with constant coefficients. Here, the RK4 method is introduced to demonstrate the numerical performance of the proposed technique. Equation (6) can then be expressed as[23]

$$\phi(x,t+dt)=\phi(x,t)-K_{\mathrm{RK4}}\hat{H}_D dt, \tag{16}$$

where K_{RK4} is called the modified coefficient vector, which can be calculated by

$$K_{\mathrm{RK4}}=\phi(x,t)\left[1-\tfrac{1}{2}\hat{H}_D dt+\tfrac{1}{6}\hat{H}_D^2 dt^2-\tfrac{1}{24}\hat{H}_D^3 dt^3\right]. \tag{17}$$

The RK4 method retains only the first four terms in the Taylor expansion, while the Euler method keeps the first term $\phi(x,t)$ in the Taylor expansion. The stability criterion using the Chebyshev–Fourier method, especially its convergence property, has been extensively discussed by Peng and Pan.[20] Euler and RK4 are well-established methods, which have been extensively presented in the literature.[24] The stability criteria of these methods mainly depend on the time step size and the absolute maximum eigenvalue $|\lambda_{\max}|$ of the system operator $\hat{H}_D$. For the Euler method $\phi(x,t+dt)=\phi(x,t)(1-\hat{H}_D dt)$, the stability is ensured when $|I+\lambda_i(-\hat{H}_D dt)|<1\,\forall\, i$, where $\lambda_i(\hat{H}_D)$ denotes the ith eigenvalue of $\hat{H}_D$. Similarly, the stability of the RK4 method is governed by $|I+\lambda_i(-\hat{H}_D dt)+\lambda_i^2(-\hat{H}_D dt)/2+\lambda_i^3(-\hat{H}_D dt)/6+\lambda_i^4(-\hat{H}_D dt)/24|<1\,\forall\, i$. Detailed discussions will be given in Sec. IV. However, the fatal drawback of the Euler and RK4 methods is that the associated numerical error is usually proportional to the time step used in the simulation. This often leads to significant accumulated error in both the magnitude and the phase of the acoustical wave in propagation. The above-mentioned drawback can be further demonstrated by comparing its calculated result with those obtained by the Chebyshev polynomial expansions based on a simple function $f(t)=e^{-t}$. Here, it is necessary to explicitly mention that there are two Chebyshev polynomial expansions (interpolation and extrapolation) to obtain the approximation results. Actual analysis errors not only include truncation errors due to interpolation or extrapolation, but also the stability effects. More details about Chebyshev polynomial expansions for this function can be found in the Appendix.

The main attention does not focus on the high numerical accuracy provided that the extremely small time step is chosen. On the contrary, there is increasing interest in the use of a very long time step, even just one step to complete the calculation for some specific problems. As shown in Fig. 2, the Chebyshev polynomial expansion has much better accuracy for a larger time step, which has the most important effect on computational efficiency, in particular the three-dimensional structure calculations. An important observation is that the Chebyshev polynomial interpolation expansion agrees well with the Chebyshev polynomial extrapolation expansion (AWP Chebyshev) for both cases when $n=4$ and $n=10$. For the Chebyshev methods, when the order of the expansion terms n increases, there are more Chebyshev nodes with higher accuracy. As shown in Fig. 2, the curves go up in value and down to another Chebyshev interpolation node again. An overwhelming performance is that the approximation error nearly keeps the same order from the first iteration to the last iteration. For the RK4 method, the curve is nearly symmetrical to the central position $t=0$. As the absolute value of t increases, the approximation accuracy deteriorates exponentially. It is the reason that only very small time steps can be adopted and the number of steps required for modeling a complete propagation is large. On the other hand, irrespective of orders used, for a long-term calculation the final result will be divergent. The Chebyshev

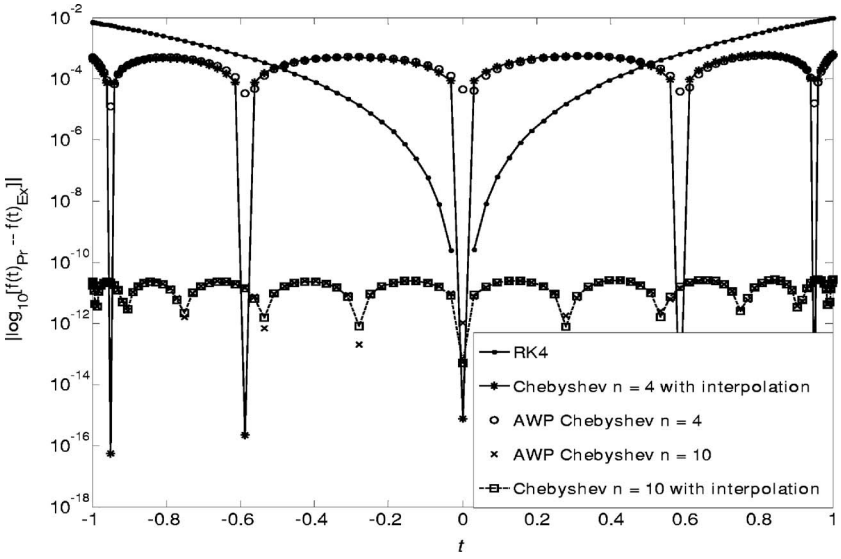

FIG. 2. Absolute errors of the RK4, fourth and tenth Chebyshev polynomial interpolation and extrapolation methods compared with the exact solutions for the function $f(t)=e^{-t}$ based on the variable time-step sizes (the subscripts Pr and Ex represent prediction and exact results).

polynomial expansion overcomes this fatal disadvantage. The calculation is still convergent even when the time is nearly infinite provided that the calculation parameters are properly chosen, such as the time step, the number of grid points, and the order of the Chebyshev polynomial expansion terms.

D. The mapped Chebyshev method

The above-presented Lagrange–Chebyshev interpolation polynomials are different from the traditional Chebyshev pseudospectral method: The following Chebyshev polynomials are used to implement the AWP by $[I_0(R)I+2I_1(R)\hat{H}'_D+2\Sigma_{n=2}^{\infty}I_n(R)T_n(\hat{H}'_D)]$ or $\Sigma_{m=0}^{M}\beta_m J_m(R)\tilde{T}_m(\hat{H}'_D)$. Therefore, the spatial differentiation matrix d_χ is included in $\hat{H}'_D$. In particular, the matrix d_x is not a well-behaved one with eigenvalues scattered in the left-hand side of the complex plane. While most of the eigenvalues grow like $O(N)$, a few of them are $O(N^2)$. This is the reason why, for a traditional Chebyshev pseudospectral method, Δt should be well below $O(N^{-2})$ so that the time marching scheme (the RK4 and Euler methods) will stay in the stable domain. Furthermore, different from the uniform grid size, for Chebyshev–Gauss–Lobatto points, the minimum grid interval $\Delta\chi_{\min}=|\chi_0-\chi_1|=1-\cos(\pi/N)=O(N^{-2})$, which is an important influential factor in choosing the time step. Here, a modified Chebyshev pseudospectral method (also called the mapped Chebyshev method) in Ref. 16 is introduced to keep both the appealing feature in time discretization and original advantage of Lagrange–Chebyshev interpolation polynomial method (for space discretization), and to improve the restrictive stability condition of the former. As a result, the computational efficiency for the previous Lagrange–Chebyshev interpolation polynomials will be improved to some extent. Based on this motivation, a brief introduction of this modified Lagrange–Chebyshev interpolation polynomials is given in the following.

Chebyshev–Gauss–Lobatto points are highly dense near the boundaries with minimal spacing. Since the pseudoespectral method is global, there is no direct relationship between the minimal spacing and the stability condition as in the finite-difference method. However, numerical experience shows that the superfine grid near the boundaries leads to the severe stability condition. Therefore, sharp gradients exist near the boundaries, the highly dense points are needed for resolution and the smaller time step is also needed for physical reason. To overcome the above-noted numerical difficulty, a transform algorithm is applied to map these Chebyshev–Gauss–Lobatto points χ_i to another set of points X_i in the same range $[-1,1]$. Of course, they can be redefined on any original finite internal $[x_0,x_N]$ by means of a linear transform of variable X which maps $[-1,1]$ onto $x\in[x_0,x_N]$, which is discretized at the modified Chebyshev–Gauss–Lobatto points of $X_i=\arcsin(\gamma\chi_i)/\arcsin(\gamma)$, where $\gamma\in]0,1[$ is an optimal parameter; and the notation $[0,1]$ denotes a range, excluding the two end values 0 and 1. Similarly, when $N+1$ grid points in X axis are given, according to the relations between $X\in[-1,1]$ and $x\in[x_0,x_N]$, $\partial\tilde{p}/\partial x$ can be obtained by multiplying the above-noted $\partial\tilde{p}/\partial X$ with the constants $2/(x_N-x_0)$. Differences among $\partial\tilde{p}/\partial x$, $\partial\tilde{p}/\partial\chi$, $\partial\tilde{p}/\partial X$ and three coordinates x (structural coordinate), χ (the coordinate transform with the Chebyshev–Gauss–Lobatto points), and X (the coordinate transform with these modified Chebyshev–Gauss–Lobatto points) should be noted.

The minimal spacing near the boundaries is stretched with larger minimal spacing,

$$X_i=\Re(\chi_i,\gamma). \tag{18}$$

As a result, this mapped method not only reduces the roundoff error but also requires less calculated points compared with previous Lagrange–Chebyshev interpolation polynomials.

Similarly, the spatial derivative of this new function can be obtained by the chain rule,

$$\Re'(\chi_i,\gamma)=\frac{\gamma}{\arcsin(\gamma)\sqrt{1-\gamma^2\chi_i^2}}. \tag{19}$$

Thus, the values at the new grid points $X_i=\Re(\chi_i,\gamma)$, $i=0,1,\ldots,N$ can be calculated by

TABLE I. The effect of N on the parameters $\kappa, \gamma, \underbrace{\Delta X_{\min}(\varepsilon,N)}_{0<\gamma<1}, \underbrace{\Delta X_{\min}(\gamma,N)}_{\gamma\to 0}, \underbrace{\Delta X_{\min}(\gamma,N)}_{\gamma\to 1}$.

N	γ	$O(N^{-2})$	$\Delta X_{\min}(\varepsilon,N)$	$\underbrace{\Delta X_{\min}(\gamma,N)}_{0<\gamma<1}$	$\underbrace{\Delta X_{\min}(\gamma,N)}_{\gamma\to 0}$	$\underbrace{\Delta X_{\min}(\gamma,N)}_{\gamma\to 1}$	$\frac{\Delta X_{\min}(\gamma,N)}{\Delta X_{\min}(0,N)}$	$\frac{\Delta X_{\min}(\gamma,N)}{\Delta X_{\min}(1,N)}$
1	$2.0\times10^{-16}\to0$	1×10^{0}	8.53×10^{-2}	2×10^{0}	2×10^{0}	2×10^{0}	1.0	1.0
2	$2.0\times10^{-8}\to0$	2.5×10^{-1}	4.26×10^{-2}	1×10^{0}	1×10^{0}	1×10^{0}	1.0	1.0
4	$2.0\times10^{4}\to0$	6.25×10^{-2}	2.13×10^{-2}	2.929×10^{-1}	2.929×10^{-1}	5×10^{-1}	1.0	0.5858
8	$2.0\times10^{-2}\to0$	1.56×10^{-2}	1.07×10^{-2}	7.61×10^{-2}	7.61×10^{-2}	2.5×10^{-1}	1.0	0.3044
16	$1.98\times10^{-1}\to0$	3.9×10^{-3}	5.3×10^{-3}	1.95×10^{-2}	1.92×10^{-2}	1.25×10^{-1}	1.0156	0.156
32	$5.75\times10^{-1}\to0$	9.7656×10^{-4}	2.7×10^{-3}	5.5×10^{-3}	4.8×10^{-3}	6.25×10^{-2}	1.1458	0.088
64	$8.545\times10^{-1}\to0$	2.4414×10^{-4}	1.3×10^{-3}	1.9×10^{-3}	1.2×10^{-3}	3.13×10^{-2}	1.5833	0.0607
128	$9.6\times10^{-1}\to0$	6.1035×10^{-5}	6.6620×10^{-4}	8.0093×10^{-4}	3.0118×10^{-4}	1.56×10^{-2}	2.6593	0.0513
256	$9.897\times10^{-1}\to0$	1.5259×10^{-5}	3.3310×10^{-4}	3.6411×10^{-4}	7.5298×10^{-5}	7.8×10^{-3}	4.8356	0.0467
512	$9.974\times10^{-1}\to0$	3.8147×10^{-6}	1.6655×10^{-4}	1.7354×10^{-4}	1.8825×10^{-5}	3.9×10^{-3}	9.2196	0.0445
1024	$9.994\times10^{-1}\to1$	9.5367×10^{-7}	8.3275×10^{-5}	8.8227×10^{-5}	4.7062×10^{-6}	2×10^{-3}	18.7470	$0.0441\to0.0426$

$$\frac{\partial\tilde{p}}{\partial X}=\underbrace{\aleph d_{\chi}}_{d_X}\tilde{p}, \tag{20}$$

where the diagonal matrix $\aleph$ has elements $\aleph_{i,i}=\arcsin(\gamma)\sqrt{1-\gamma^2\chi_i^2}/\gamma$. For simplicity, a new differentiation matrix d_X is defined as the product of $\aleph$ and d_χ.

The parameter γ effectively balances between the accuracy associated with the Chebyshev method and improved stability of the Fourier method. To obtain an effective computation, the parameter γ must be carefully chosen. It should be noted that the parameter γ has significant impact on $\aleph_{i,i}$, $\partial\tilde{p}/\partial X$ and subsequently on the prediction result of the sound pressure $\tilde{p}$. When $\gamma\to0$, $\aleph_{i,i}=\arcsin(\gamma)\sqrt{1-\gamma^2\chi_i^2}/\gamma=\arcsin(\gamma)/\gamma\to1$, the minimal spacing $\Delta X_{\min}=1-\cos(\pi/N)$ is the same as in standard Chebyshev methods $\Delta\chi_{\min}$. However, it is worth noting that, $\gamma\in\,]0,1[$ is an optimal parameter, excluding the two end values 0 and 1. In other words, γ can only indefinitely come nearer to 1, but not $\gamma=1$. It means that $d_X=d_\chi$, the mapped method does not reach its original target. When $\gamma\to1$, $\aleph_{i,i}=\arcsin(\gamma)\sqrt{1-\gamma^2\chi_i^2}/\gamma=\pi\sin(i\pi/N)/2$, the minimal spacing

$$\Delta X_{\min}=|X_{N-1}-X_N|=\underbrace{\left|\arcsin(\gamma\chi_{N-1})/\arcsin(\gamma)-1\right|}_{\gamma\to1}$$
$$=|2\arcsin(\cos(\pi/N))/\pi-1|=2/N,$$

which is the same order as the uniform spacing (Fourier case) Δx $(O(L_x/N))$. In other words, the restriction on the time step related to the stability condition has been removed.

According to the previously defined range, the parameter γ can be expressed as $\gamma=(N^2-\kappa^2)/N^2$, where $\kappa\in\,]0,N[$, while excluding the two end values: 0 and N. Then the minimal spacing $\Delta X_{\min}=2\pi/(N(\sqrt{\pi^2+2\kappa}+\sqrt{2\kappa}))$. When $\kappa=|\ln\varepsilon|^2/2$ and $\gamma=\operatorname{sech}(|\ln\varepsilon|/N)$, the approximation error (the accuracy) is close to ε, which is the machine precision of the computer.

Thus, the minimal spacing $\Delta X_{\min}$ can be calculated by

$$\Delta X_{\min}=\frac{1}{\sqrt{1+|\ln\varepsilon|^2/\pi^2}+\sqrt{|\ln\varepsilon|^2/\pi^2}}\frac{2}{N}\cong\frac{\pi}{N|\ln\varepsilon|}. \tag{21}$$

When ε is fixed, $\Delta X_{\min}$ is only a function of N.

Table I shows the effect of the number of the modified Chebyshev–Gauss–Lobatto points on the parameters

$$\kappa,\gamma,\underbrace{\Delta X_{\min}(\varepsilon,N)}_{0<\gamma<1},\underbrace{\Delta X_{\min}(\gamma,N)}_{\gamma\to0},\underbrace{\Delta X_{\min}(\gamma,N)}_{\gamma\to1},\Delta X_{\min}(\gamma,N)/\Delta X_{\min}(0,N)\text{ and }\Delta X_{\min}(\gamma,N)/\Delta X_{\min}(1,N).$$

As shown in the second column, the value of γ changes from 0 to 1 as the number N increases from 1 to 1024. The ratios in the eighth and ninth columns demonstrate the effect of the different values of γ on $\Delta X_{\min}(\gamma,N)$, which is directly related to the time step selected (computational efficiency).

IV. NUMERICAL EXAMPLES AND RESULTS

A. Numerical examples and exact analytical solutions for periodic and nonperiodic boundary conditions

First of all, to demonstrate the above-presented methods, the following modified Gaussian impulse is selected as the initial wave packet with corresponding boundary conditions:

$$p(x,0)=f(x)=0.04^2x^2(x-x_N)^2\exp\left(-\left[\frac{(x-x_c)^2}{4\sigma^2}\right]\right),$$

$$\frac{\partial p(x,0)}{\partial t}=g(x)=0, \tag{22}$$

and

$$\frac{\partial p(x_0,t)}{\partial x}=\frac{\partial p(x_N,t)}{\partial x}=0, \tag{23}$$

where x_c and σ denote the position and Gaussian factor of the initial wave packet, respectively; and to ensure the maximum initial value with positive unit, the sound pressure and its first-order spatial derivative with zero at two ends, the

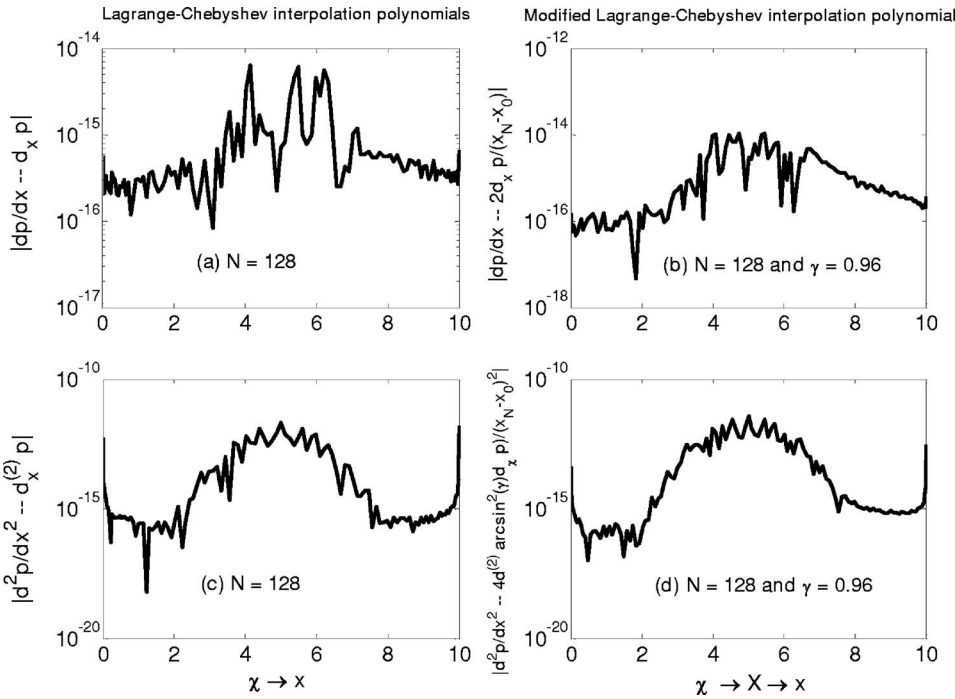

FIG. 3. The first-order and second-order derivatives of sound pressure with Lagrange–Chebyshev interpolation polynomial and modified Lagrange–Chebyshev interpolation polynomial methods.

constant (0.04^2), the terms x^2 and $(x-x_N)^2$ are introduced, respectively.

The exact solution of the sound pressure $p(x,t)=[f(x+ct)+f(x-ct)]/2$ is used for the purpose of comparison. The integral coefficients can be evaluated numerically by numerical integration using MATLAB functions. When $N=16$, the approximation error is the order $O(10^{-14})$, which is the same as that of the specified quadrature accuracy $\delta=1\times10^{-14}$. However, due to the few points used, the curve is not smooth. As N increases ($N\geqslant128$), the approximation error and its variation trend becomes stable. Therefore, the following numerical calculations use $N=128$.

B. Analysis of numerical accuracy and computational efficiency

For the AWP method implementation as in Ref. 20, the Fourier transform scheme was adopted to evaluate the spatial derivative such as $\hat{p}_x=F[\partial p/\partial x]=(jk)F[p(x,t)]=(jk)\hat{p}$, where $\hat{p}$, $\hat{p}_x$, k, and $F[\ ]$ represent the sound pressure and its spatial derivative in the wave number domain, the wave number along the x axis, and the Fourier transform, respectively. Then the inverse Fourier transform is applied to get $\partial p(x,t)/\partial x=F^{-1}\{\hat{p}_x\}$.

For the above-mentioned initial-value problems with nonperiodic boundary condition [a hard wall with $\partial p(x_0,t)/\partial x=0$ imposed on the left-hand side and a pressure-release wall with $p(x_N,t)=0$ imposed on the right-hand side], the Lagrange–Chebyshev interpolation polynomial method with modified Chebyshev–Gauss–Lobatto points is used for calculating the spatial derivatives. Here, only two spatial derivatives $\partial p(x,t)/\partial x$ and $\partial^2 p(x,t)/\partial x^2$ are demonstrated to evaluate this new feature.

The exact solutions of the first-order and second-order derivatives are given by

$$\frac{\partial p(x,t)}{\partial x}=\sum_{m=0}^{\infty}[-c_m\eta_m\sin(\eta_m x)\cos(\zeta_m t)],$$

$$\frac{\partial^2 p(x,t)}{\partial x^2}=\sum_{m=0}^{\infty}[-c_m\eta_m^2\cos(\eta_m x)\cos(\zeta_m t)], \tag{24}$$

where $\eta_m=(m+1/2)\pi/L_x$ and $\zeta_m=c_0(m+1/2)\pi/L_x$.

According to Eq. (22), $f'(x)$,$f''(x)$ can be obtained by

$$f'(x)=\frac{\partial p(x,0)}{\partial x}=0.04^2\left[2x(x-x_N)(2x-x_N)-x^2(x-x_N)^2\frac{(x-x_c)}{2\sigma^2}\right]\exp\left(-\left[\frac{(x-x_c)^2}{4\sigma^2}\right]\right),$$

$$f''(x)=\frac{\partial^2 p(x,0)}{\partial x^2}=0.04^2\left[12x^2-12xx_N+2x_N^2-\frac{(x-x_N)(9x^3-8x^2x_c+4xx_Nx_c-5x^2x_N)}{2\sigma^2}+x^2(x-x_N)\frac{(x-x_c)^2}{4\sigma^4}\right]\exp\left(-\left[\frac{(x-x_c)^2}{4\sigma^2}\right]\right). \tag{25}$$

Figure 3 shows the comparison of the prediction results by the Lagrange–Chebyshev method [(a) $dp/d\chi=d_\chi p$ and (b) $d^2p/d\chi^2=d_\chi^{(2)}p$]; the modified Lagrange–Chebyshev method [(c) $dp/dX=\aleph d_\chi p$ and (d)

$$d^2p/dX^2=d(dp/dX)/dX=\aleph d_\chi(dp/dX)+d_\chi(d\aleph/dX)p=\underbrace{\aleph^2 d_\chi^{(2)}p}_{d_\chi^{(2)}}-\underbrace{\arcsin^2(\gamma)\chi}_{\tilde{d}_\chi^{(1)}}\underbrace{d_\chi p}_{dp/d\chi}$$

and the exact expressions for the initial wave packet given in Eq. (22), where $\aleph^2$ is the square of the diagonal matrix $\aleph$ and

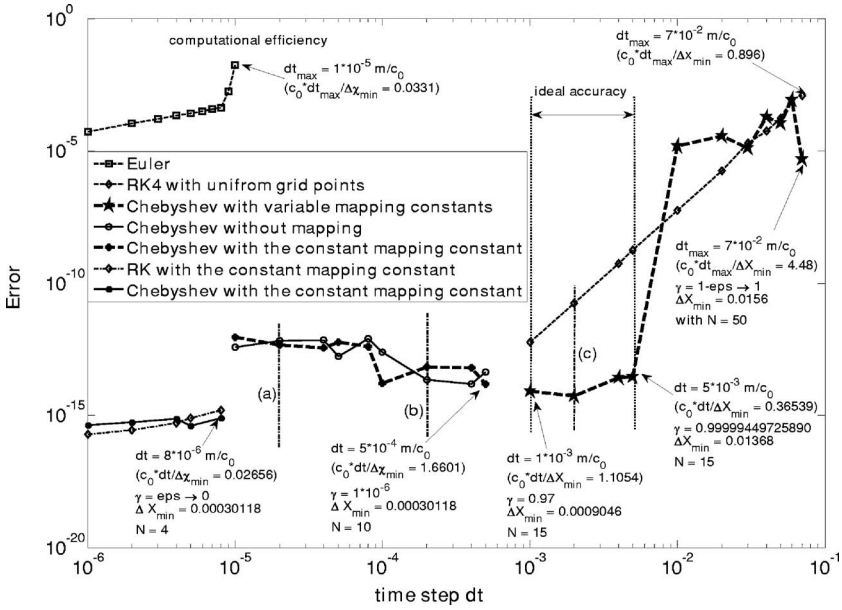

FIG. 4. Errors of the Euler, RK4, and AWP methods with/without the mapped Chebyshev method compared to the exact solutions in different time steps.

$\tilde{d}_x^{(1)}$ is the diagonal matrix with entries $\tilde{d}_{X_{ii}}^{(1)} = \Re''(\chi_i,\gamma)/(\Re'(\chi_i,\gamma))^3 = \arcsin^2(\gamma)\chi_i$. For the first-order and second-order derivatives, the maximum errors of the Lagrange–Chebyshev interpolation polynomial method are 6.3283×10^{-15} and 2.0970×10^{-12}, respectively. For the present modified Lagrange–Chebyshev interpolation polynomial method, as shown in Figs. 3(c) and 3(d), the maximum errors have slightly increased to 1.088×10^{-14} and 3.7788×10^{-12}, respectively. Therefore, the above-presented analysis demonstrates that the modified Lagrange–Chebyshev method keeps the high accuracy for calculating the spatial derivatives. Later discussion will also show that the computational efficiency is also greatly improved at the same time.

The sound pressure inside the duct is calculated hereafter. The main parameters used in this computation are given as follows: The speed of sound $c_0=344$ m/s, the structure sizes are $x_0=0$ m, $x_N=10$ m, $x_c=5$ m, and $\sigma=0.5$. Figure 4 shows the error comparison between the Euler method, the RK4 method, and the Chebyshev method with/without the mapped Chebyshev method. It also shows the effect of γ in the mapped Chebyshev method on the prediction results, in particular the numerical accuracy and computational efficiency. Due to the nonuniform Gauss–Lobatto points, the traditional error evaluation methods (the maximum absolute error, root mean square) are not appropriate. In what follows, the error is defined as the difference between the calculated results and exact results in terms of $\int_{x_0}^{x_N} p(x,t)dx$, where x_N and x_0 represent the upper and lower limits of integration. To this end, the multiple-application trapezoidal rule is used for integration due to the unequal segments ($dx \neq L_x/N$). For discussion purposes, the size of the time step used can be roughly divided into three zones: (a) Small time step $dt \in [1\times10^{-6}, 1\times10^{-5}]m/c_0$; (b) moderate time step $dt \in [1\times10^{-5}, 1\times10^{-3}]m/c_0$; and (c) large time step $dt \in [1\times10^{-3}, 7\times10^{-2}]m/c_0$.

Euler method can only be used in zone one, which requires a very small time step ($dt_{\text{Euler}}=1\times10^{-6}m/c_0$). In particular, as the size of the time step increases, the approximation errors increase linearly. Beyond a certain critical value of $dt=8\times10^{-6}m/c_0$ ($c_0dt/\Delta X_{\min}=0.02648$), the error increases dramatically and the calculation becomes divergent. Overall speaking, the accuracy of the Euler method, even within its validity zone, is still significantly lower compared to other methods. In the same zone, the Chebyshev methods with/without mapping do not show any noticeable difference (not shown in Fig. 4). Figure 4 shows that, in this particular zone, the RK4 method and Chebyshev methods provide comparable calculation accuracy. Generally speaking, as the size of the time step increases, the approximation errors obtained by both methods increase roughly in a linear pattern.

In zone two with moderate time steps, the Chebyshev methods with/without mapping are shown to demonstrate the effect of γ on the calculation errors. The impact of performing mapping starts to be obvious. With the increase of the time step, error curves do not necessarily undergo monotonous increase, suggesting a possible optimization on the combination of the expansion term n and γ to achieve high numerical accuracy.

The effect of the uniform grid points and Chebyshev–Gauss–Lobatto points (especially the modified Chebyshev–Gauss–Lobatto points by the mapped Chebyshev method) on the numerical accuracy and computational efficiency can be clearly seen in zone three. Within this zone, it is observed that the previous Lagrange–Chebyshev method without the mapped Chebyshev method or any higher-order RK methods (>4) fail to provide converged results. Therefore, Fig. 4 only compares the proposed method to the RK4 method with the uniform grid points. Figure 4 shows that the maximum time step allowed by modified Chebyshev–Gauss–Lobatto points by the mapped Chebyshev method can be up to $dt_{\max}=7.0\times10^{-2}m/c_0$ ($c_0dt_{\max}/\Delta x_{\min}=0.896$). Within this zone, however, there exists an optimal range in which modified Chebyshev–Gauss–Lobatto points by the mapped Chebyshev method outperforms the RK4 method by providing a much better accuracy for the same time step used. This range can be determined by properly choosing the expansion term n

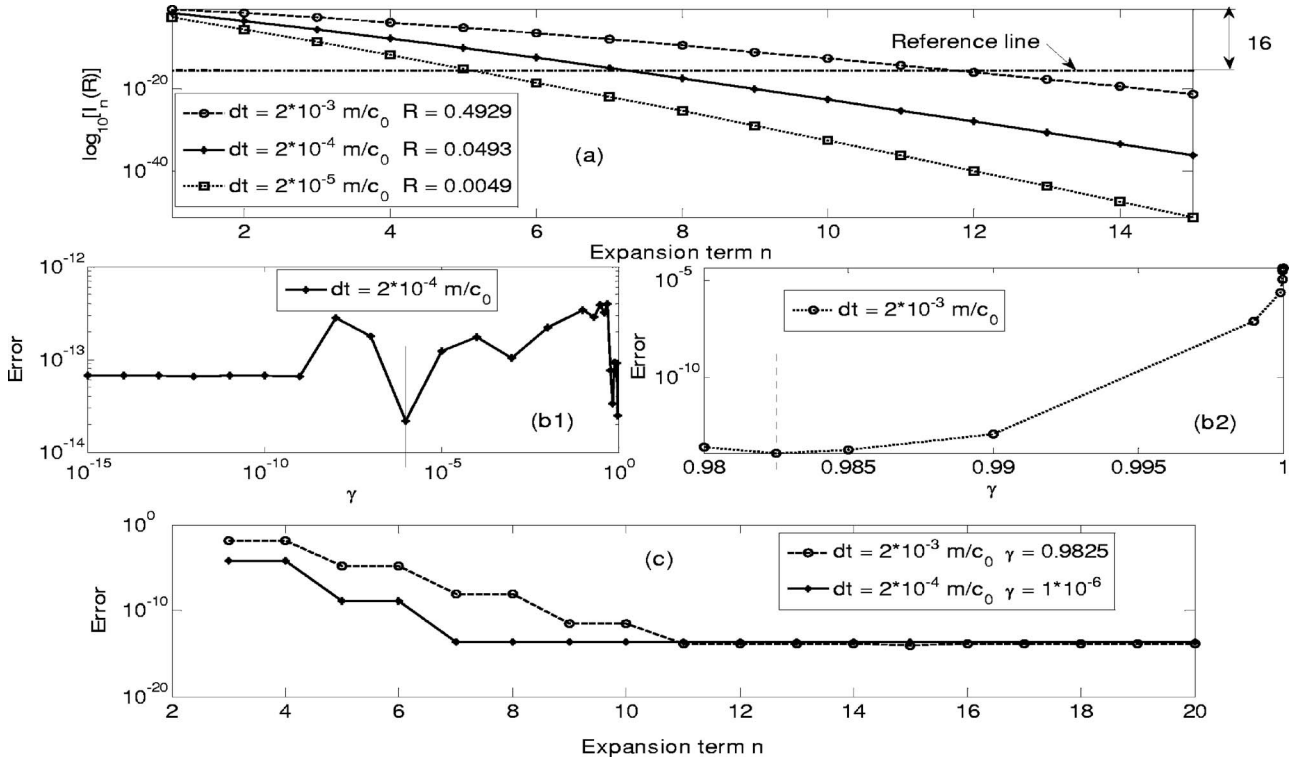

FIG. 5. Effects of the expansion term n and γ on the prediction error.

and γ, such as the following two sets of combinations: (1) $dt=1.0\times10^{-3}m/c_0$ with $\gamma=0.97$ and $n=15$ and (2) $dt=5.0\times10^{-3}m/c_0$ with $\gamma=0.99999449725890$ and $n=15$, as shown in the right-hand lower corner of Fig. 4. Therefore, the proposed technique allows the use of relatively large time steps while maintaining the good calculation accuracy, in which circumstance all other investigated methods fail.

An appealing feature of the Chebyshev polynomial method lies in its ability to prevent accumulation of the truncation errors. Given a time step, the RK method, however, accumulates the truncation error as the selected expansion term increases. It is the reason why both the Euler and RK4 methods are not quite suitable for a long-term calculation. For the same reason, only lower-order RK methods are widely used. The above-presented analysis shows that the modified AWP scheme (double Chebyshev methods both in temporal operator and spatial derivatives) has much better performance in terms of both numerical accuracy and computational efficiency due to the use of larger time step.

The allowable maximum time step $dt_{\max}$ is a crucial parameter governing the numerical accuracy and computational efficiency, as shown in Fig. 4. The effect of the expansion term n and γ on the calculation error based on the modified Lagrange–Chebyshev method with the mapped Chebyshev method is investigated. Three typical time steps are selected from each of the three zones mentioned earlier (Fig. 4): (a) $dt=2.0\times10^{-5}m/c_0$; (b) $dt=2.0\times10^{-4}m/c_0$; and (c) $dt=2.0\times10^{-3}m/c_0$, respectively. The number of the expansion term n in the Chebyshev method is first examined in terms of the coefficients of the first kind of Bessel function $I_n(R)$. Currently, the state-of-the-art computer provides a dynamic range of about 10^{-16}. We attempt to determine the minimum expansion terms needed to ensure that the truncation errors do not contribute to the final result and the sum of the polynomials converges to the order of $I_{n_{\min}}(R)$. The convergence properties of $I_n(R)$ for three given R values (0.0049, 0.0493, 0.4929) calculated from the three time steps mentioned earlier are illustrated in Fig. 5(a). It can be seen that $I_n(R)$ decreases monotonically with the increase of n. For a threshold value $I_0(R)/I_{n_{\min}}(R)=10^{16}$, there exists a minimum value of $n(n_{\min})$. Small R corresponds to a small $n_{\min}$. With a reference line defined by $|\log_{10}^{I_{\text{ref}}(R)/I_0(R)}|=16$, Fig. 5(a) shows that $n_{\min}$ takes the value of 4, 6, and 10 for $R=0.0049$, 0.0493, and 0.4929, respectively. For safety's sake, however, we use $n=10$ and 15 for $R=0.0493$ and 0.4929, respectively. Furthermore, when R takes other values within the range of 0.0049–0.4929, corresponding $n_{\min}$ value can be estimated by interpolation using Fig. 5(a).

The effect of γ on the prediction error is shown in Figs. 5(b1) and (b2), using two time steps ($dt=2.0\times10^{-4}m/c_0$, $dt=2.0\times10^{-3}m/c_0$). With a moderate time step $dt=2.0\times10^{-4}m/c_0$, Figure 5(b1) shows that γ has no effect on the calculation error when its value is small enough ($<1\times10^{-9}$). As γ further increases, γ shows strong influence on the calculation error with several "local minima," suggesting a possible optimization on γ to achieve the highest computation accuracy. Generally speaking, with this γ range (from $\gamma=1\times10^{-15}$ to $\gamma\to1$), the prediction results are found to be highly accurate [the order of error below $O(10^{-12})$]. With a larger time step $dt=2.0\times10^{-3}m/c_0$, Fig. 5(b2) shows that the prediction error remains rather low [$O(10^{-12})$] within a very narrow range from $\gamma=0.98$ to $\gamma=0.985$. Exceeding this range, the prediction accuracy rapidly deteriorates and the

calculation error increases drastically with the increase of γ. The above-presented analysis demonstrates that constant $\gamma = 1$ is not a good choice. Therefore, the value of γ needs to be carefully chosen in order to ensure the accuracy, or even the convergence of the calculation. When the time step dt and the parameter γ are fixed, the effect of the expansion term n on the prediction error is also shown in Fig. 5(c). It can be seen that, as n increases, the prediction error gradually improves until a certain value.

V. CONCLUSIONS

An AWP technique with the mapped Chebyshev method is proposed to describe the time-domain evolution of acoustical waves. Using a numerical example in a duct structure, the numerical accuracy, computational efficiency, and stability of the technique are investigated, leading to the following conclusions:

(1) Drawbacks and limitations of fast Fourier transform and the existing Chebyshev–Fourier scheme in dealing with nonperiodic boundaries are surmounted by the proposed combined scheme: A Chebyshev polynomial expansion scheme in the temporal AWP operator and the modified Lagrange-Chebyshev interpolation polynomials scheme with the mapped Chebyshev method in the spatial derivatives evaluation. The latter not only keeps the high accuracy for calculating the spatial derivatives, but also significantly improves the computational efficiency. Meanwhile, a mathematical model with nonperiodic boundary conditions is introduced in the spatial derivatives, allowing the consideration of any boundary conditions.
(2) For large R values, the J expansion is better because large prediction errors can be avoided when some extra terms fall outside of the dynamic range defined by the machine accuracy of the computer (10^{-16}). For small R values, the previous I expansion is recommended due to its exponential decaying property.
(3) The time step restriction due to the high-density grid near the boundaries with minimal spacing has been overcome by introducing the mapped Chebyshev method. Three zones are observed in which the proposed method shows different characteristics with respect to other existing methods. In zone one with very small time steps, the Chebyshev methods with/without mapping do not show any noticeable difference. Apart from the Euler method, other conventional numerical methods studied in this paper provide very comparable numerical accuracy. In zone two with moderate time steps, the effect of γ (is an optimal parameter $\gamma \in]0,1[$, excluding the two end values 0 and 1) on the Chebyshev methods with mapping is obvious. With the increase of the time step, error curves do not necessarily undergo monotonous increase, suggesting a possible optimization on the combination of the expansion term n and γ to achieve high numerical accuracy. In zone three with large time steps, γ dominates the numerical accuracy and computational efficiency. By properly choosing the expansion term n and γ, an optimal result with high numerical accuracy and computational efficiency with much larger time step used can be obtained. In this time step zone, neither the previous Lagrange–Chebyshev method without the mapped Chebyshev method nor the high–order RK methods can be used.

The numerical analyses carried out in this paper demonstrate that the modified Lagrange–Chebyshev method with the mapped Chebyshev method can satisfactorily handle the nonperiodic boundary conditions and initial-value problems. The proposed method provides a good combination of numerical accuracy, computational efficiency, and stability, in particular for long-term calculations. The work presented in this paper provides significant improvement to the existing AWP method, opening doors to a large number of engineering problems. Typical examples may include problems involving fluid–structural interactions and physical systems exhibiting strong nonlinear behavior. The framework established in this paper allows straightforward extension to the first type of problems, while the second one is much more challenging and requires further in-depth investigations.

ACKNOWLEDGMENTS

The authors are grateful to Dr. L. Huang for his help in numerical analysis, especially his original contribution to the Lagrange–Chebyshev method developed for the nonperiodic boundary condition. The authors also benefited from valuable discussions with Professor J. Pan and Dr. K. S. Sum. S.Z.P. is thankful for financial support from the Postdoctoral Fellowship Scheme of the Hong Kong Polytechnic University (G-YX62).

APPENDIX: THE RK4 METHOD FOR A SIMPLE FUNCTION $F(T)=E^{-T}$

For the function $f(t)=e^{-t}$, there are two kinds of Chebyshev polynomial expansions: (a) Interpolation approximation and (b) extrapolation expansions. For the former, the Chebyshev polynomial expansion $f_{\mathrm{Ch}}(t)$ of degree n for $f(t)$ over the interval $[-1,1]$ can be written as a sum of $T_j(t)$:

$$f(t) \approx f_{\mathrm{Ch\_Inter}}(t) = \sum_{j=0}^{n} c_j T_j(t). \tag{A1}$$

The coefficients c_j are computed with the following formulas:

$$c_0 = \frac{1}{n+1}\sum_{k=0}^{n} f(t_k)T_0(t_k) = \frac{1}{n+1}\sum_{k=0}^{n} f(t_k); \quad c_1 = \frac{2}{n+1}\sum_{k=0}^{n} f(t_k)T_1(t_k) = \frac{2}{n+1}\sum_{k=0}^{n} f(t_k)t_k \tag{A2}$$

and

$$c_j = \frac{2}{n+1}\sum_{k=0}^{n} f(t_k)T_j(t_k) = \frac{2}{n+1}\sum_{k=0}^{n} f(t_k)(2t_k T_{j-1}(t_k) - T_{j-2}(t_k)), \tag{A3}$$

where $j=2,\ldots,n$ and t_k denote the Chebyshev interpolation nodes calculated by $t_k=-\cos((2k+1)\pi/(2n+2))$ for $k=0,1,2,\ldots,n$. Strictly speaking, the coefficients c_j are obtained by borrowing the future results of the function $f(t_k)$, as shown in Eq. (A3).

Thus, when $n=4$ (taken the same terms as that in the RK4 method), Eq. (A1) can be given by

$$\begin{aligned} f_{\text{Ch4\_Inter}}(t) = {} & \underbrace{1.2660658}_{c_0} - \underbrace{1.1303182}_{c_1}t + \underbrace{0.2714951}_{c_2}(2t^2 - 1) - \underbrace{0.0443337}_{c_3}(4t^3 - 3t) + \underbrace{0.0054293}_{c_4}(8t^4 - 8t^2 + 1) \\ = {} & 1.0 - 0.9973173t + 0.4995562t^2 - 0.1773346t^3 + 0.0434341t^4. \end{aligned} \tag{A4}$$

For the latter,

$$f(t) \approx f_{\text{Ch}}(t) = \left[I_0(R)T_0\left(\underbrace{t-t_0}_{\hat{H}'}\right) + 2I_1(R)T_1(t-t_0) + \sum_{m=2}^{M} 2I_m(R)T_m(t-t_0) \right] f(t_0),$$

where $I_m(R)$ is the mth-order Bessel function of the first kind. This simple function $f(t)=e^{-t}$ can be simplified from $f(t)=e^{-R\hat{H}'}$ provided that $R=1$, $\hat{H}'=t-t_0$ and $t_0=0$. $T_0(t)=1$, $T_1(t)=t$, and the rest can be calculated by the following recursive relations: $T_{m+1}(t)=2tT_m(t)-T_{m-1}(t)$. Different from the previous interpolation expansions, it is worth noting that the coefficients $I_m(R)$ and $T_m(t)$ are calculated by known results at present time step.

[1] J. Dollimore, "Some algorithms for use with the fast Fourier transform," J. Inst. Math. Appl. **12**, 115–117 (1973).
[2] J. P. Coyette, "Transient acoustics: Evaluation of finite element and boundary element methods," Proceedings of ISMA 19, Leuven, Belgium, September 12–14, 1994, pp. 223–234.
[3] R. Renaut and J. Frohlich, "A pseudospectral Chebyshev method for the 2D wave equation with domain stretching and absorbing boundary conditions," J. Comput. Phys. **124**, 324–336 (1996).
[4] F. Q. Hu, M. Y. Hussaini, and J. L. Manthey, "Low-dissipation and low-dispersion Runge-Kutta schemes for computational acoustics," J. Comput. Phys. **124**, 177–191 (1996).
[5] Z. Jackiewicz and B. D. Welfert, "Stability of Gauss-Radau pseudospectral approximations of the one-dimensional wave equation," SIAM J. Sci. Comput. (USA) **18**, 287–313 (1996).
[6] K. Burrage and E. Platen, "High strong order explicit Runge-Kutta methods for stochastic ordinary differential equations," Appl. Numer. Math. **22**, 81–101 (1996).
[7] K. Y. Fung, "Time-domain computation of acoustics in confinements," Proceedings of the Fifth International Congress on Sound and Vibration, Adelaide, Australia, December 15–18, 1997, pp. 1839–1847.
[8] J. B. Schneider and O. M. Ramahi, "The complementary operators method applied to acoustic finite-difference time-domain simulations," J. Acoust. Soc. Am. **104**, 686–693 (1998).
[9] D. R. Hans, K. Michielsen, J. S. Kole, and M. T. Figge, "Solving the Maxwell equations by the Chebyshev method: A one-step finite-difference time-domain algorithm," IEEE Antennas Propag. Mag. **51**, 3155–3160 (2003).
[10] A. Gelb, Z. Jackiewicz, and B. Welfert, "Absorbing boundary conditions of the second order for the pseudospectral Chebyshev methods for wave propagation," SIAM J. Sci. Comput. (USA) **17**, 501–512 (2002).
[11] M. D. Feit, J. A. Fleck, and A. Steriger, "Solution of the Schrödinger equation by a spectral method," J. Comput. Phys. **47**, 412–433 (1982).
[12] N. Balakrishnan, C. Kalyanraman, and N. Sathyamurthy, "Time-dependent quantum mechanical approach to reactive scattering and related processes," Phys. Rep. **280**, 79–144 (1997).
[13] H. Tal-Ezer and R. Kosloff, "An accurate and efficient scheme for propagating the time-dependent Schrödinger equation," J. Chem. Phys. **81**, 3967–3971 (1984).
[14] R. Kosloff and D. Kosloff, "Absorbing boundaries for wave propagation problems," J. Comput. Phys. **104**, 363–376 (1985).
[15] R. Kosloff, "Time-dependent quantum-mechanical methods for molecular dynamics," J. Phys. Chem. **92**, 2087–2100 (1988).
[16] D. Kosloff and H. Tal-Ezer, "Modified Chebyshev pseudospectral method $O(N^{-1})$ with time step restriction," J. Comput. Phys. **104**, 457–469 (1993).
[17] W. S. Don and A. Solomonoff, "Accuracy enhancement for higher derivatives using Chebyshev collocation and a mapping method," SIAM J. Sci. Comput. (USA) **18**, 1040–1057 (1995).
[18] C. Leforestier, R. H. Bisseling, C. Cerjan, M. D. Feit, R. Friesner, A. Guldberg, A. Hammerich, G. Jolicard, W. Karrlein, H.-D. Meyer, N. Lipkin, O. Roncero, and R. Kosloff, "A comparison of different propagation schemes for the time domain dependent Schrödinger equation," J. Comput. Phys. **94**, 59–80 (1991).
[19] J. Pan and J. B. Wang, "Acoustical wave propagator," J. Acoust. Soc. Am. **108**, 481–487 (2000).
[20] S. Z. Peng and J. Pan, "Acoustical wave propagator for time-domain flexural waves in thin plates," J. Acoust. Soc. Am. **115**, 467–474 (2004).
[21] S. Z. Peng and J. Pan, "A study of time-domain stress concentration in a plate with sharp change of section using the acoustical wave propagator method," J. Acoust. Soc. Am. **117**, 492–502 (2005).
[22] S. Z. Peng, "Dynamic stress concentration in a ribbed plate using acoustical wave propagator method," J. Sound Vib. **279**, 75–88 (2005).
[23] S. Z. Peng and L. Huang, "The improved acoustical wave propagator method for predicting time-domain acoustical wave propagation in a duct structure," Proceedings of the Ninth Western Pacific Acoustics Conference, Seoul, Korea, June 26–28, 2006.
[24] S. C. Chapra and R. P. Canale, *Numerical Methods for Engineers* (McGraw-Hill, Boston, 2006).